

Additive Manufacturing of Magnetic Soft Materials and Magnetic Origami Robot

Thesis

Presented in Partial Fulfillment of the Requirements Graduation with Honors Research

Distinction in Department of Mechanical Engineering at The Ohio State University

By

Jize Dai

Undergraduate Program in Mechanical Engineering

The Ohio State University

2021

Thesis Committee

Ruike Zhao, Ph.D., Advisor

David Hoelzle, Ph.D.

Copyrighted by

Jize Dai

2021

## **Abstract**

The soft actuator has been using in many applications such as robotics, biochemical devices, and consumer products. Magnetic Soft Materials (MSMs) are one of the soft actuators that have functions of reversible shape transformation, untethered, fast, and shape controllable under applied magnetic fields. Magnetic shape memory polymers(M-SMPs), as one of the MSMs, have a new type of function: shape locking. With temperature changing, it can increase or decrease its Young's Modules to change its stiffness which both achieved shape-changing and energy saving. However, its thermal curing fabrication method limits its design shape only to simple geometry shapes. Here, with our photocuring method and developed multimaterial printing technology, we have designed complex structures contain both M-SMPs and MSMs. Under thermal and magnetic actuation, the complex structures are capable of shape-changing and shape locking. It accomplished multiple usages relative to different shapes in one construction. To increases the functionality of our designs, we further analyze one of the unique patterns of origami, a paper-folding art, called Kresling origami. Kresling origami contains a propeller-like structure with two stable states: deployed state and folded state. With a magnetic-responsive plate on the side of the structure, our Kresling origami robot performs a swimming motion under a rotating magnetic field. In this article, both magnetic soft material and magnetic origami robot are separately analyzed, and we believe a combination with both technologies has great potentials in biomedical applications.

## **Acknowledgments**

I wish to extend my special thanks to my advisor Dr. Zhao for providing me the chance to learn and study in the SIM laboratory and giving me multiple opportunities to improve myself. Without her active guidance and encouragement, I will not earn my success at Ohio State. Also, a special thanks to Dr. Ze, Shuai Wu, and Chunping Ma for their continually support through my research studying.

I would like to thanks all my family and friends for cheering me up that not only encourage me for overcoming all the difficulties but also gave me the courage for success.

## **Vita**

### Education

The Ohio State University  
B.S. Mechanical Engineering

2018-2021

### Awards and exhibitions and performances

MAE Outstanding Research and Leadership Award

## Table of Contents

Abstract.....	ii
Acknowledgments.....	iii
Vita .....	iv
List of Figures .....	vi
Magnetic soft materials .....	1
Introduction .....	1
Objective .....	5
Methodology.....	5
Result .....	8
Magnetic origami robot .....	13
Introduction .....	13
Methodology.....	17
Result .....	21
Conclusion.....	27
Bibliography .....	29

## List of Figures

Figure 1: Working mechanism of a cantilever made by magnetic shape memory polymer(M-SMP) <sup>1</sup> .....	2
Figure 2 Thermomechanical of M-SMP <sup>1</sup> .....	3
Figure 3 Physical property and application of M-SMP (scale bars: 5mm) <sup>1</sup> .....	4
Figure 4 Customed 3D printer for M <sup>3</sup> DIW .....	5
Figure 5 Magnetic multimaterial direct ink writing (M <sup>3</sup> DIW) <sup>2</sup> .....	6
Figure 6 Working mechanism of the multimaterial (MSM&M-SMP) <sup>2</sup> .....	7
Figure 7 Curable depth vs. UV exposure time for different NdFeB particle sizes <sup>2</sup> .....	8
Figure 8 Printing qualities for both materials with different silica loading and pressure <sup>2</sup> . 9	
Figure 9 Thermomechanical property of MSM and M-SMP <sup>2</sup> .....	10
Figure 10 The working mechanism of a 2D chiral design with MSM/M-SMP(scaler bar: 10mm) <sup>2</sup> .....	11
Figure 11 Geometry of Kresling origami .....	13
Figure 12 Magnetic actuation of the magnetic Kresling unit cell <sup>3</sup> .....	14
Figure 13 Magnetic torque vs. plate rotation angle .....	15
Figure 14 The geometry of Kresling origami (scaler bar: 5mm) .....	17
Figure 15 Magnetic Kresling robot and a right-handed propeller schematic .....	18
Figure 16 Magnetic Kresling robot with drug-release function.....	19
Figure 17 Magnetic Kresling robot swims in the horizontal direction (scaler bar: 13mm) .....	21
Figure 18 Speed vs. input frequency for different conditions for horizontal swimming .	22
Figure 19 Magnetic Kresling robot swims in the vertical direction (scaler bar: 13mm) ..	23
Figure 20 Speed vs. input frequency for different conditions for vertical swimming.....	24
Figure 21 Magnetic Kresling robot travels in maze and drug released (scaler bar: 8mm) .....	25

# Magnetic soft materials

## *Introduction*

Soft actuators have been using in many applications such as robotics, biochemical devices, and consumer products. Programmable soft materials have great potential in creating soft actuators due to their response to light, heat, or magnetic fields. By adding magnetic particles (NdFeB) into the programmable soft materials, Magnetic soft materials (MSMs) have been created that are capable of shape-changing under an external magnetic field. Shape memory polymer (SMP) is a unique type of programmable soft material that can change its stiffness under different temperatures. Researchers recently enhance its programmability by embedded magnetic particles (NdFeB) inside of SMP and named it Magnetic shape memory polymer (M-SMP). Because of SMP's unique properties, M-SMPs can achieve shape locking by controlling their temperature under an applied magnetic field. Researchers have discovered two states of the thermoresponsive M-SMP: "glassy state" and "rubbery state". The boundary that separates those two states is the M-SMP's glass-transition temperature ( $T_g$ ). When the temperature of M-SMP is lower than  $T_g$ , M-SMP stays in its "glassy state". In this state, the applied magnetic field cannot change its shape because of its high stiffness. To achieve shape-changing, M-SMP needs to be transferred to its "rubbery state" by maintaining a temperature that is higher than  $T_g$ . Researchers have discovered a method that can heat M-SMP remotely by adding  $Fe_3O_4$  particles. The  $Fe_3O_4$  particles can inductive heating under a high frequency



alternating current (AC) magnetic field which achieving temperature controllable under magnetic field.

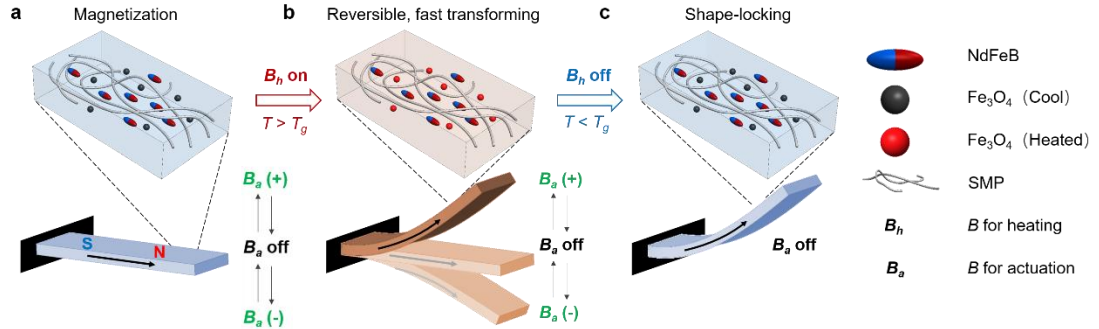


Figure 1: Working mechanism of a cantilever made by magnetic shape memory polymer(M-SMP)<sup>1</sup>

Figure 1 shows the working mechanism of a cantilever made in M-SMP. The cantilever has magnetized under an impulse magnetic field so the magnetic direction of NdFeB particles is aligned in the same direction. Under room temperature (Figure 1a), the cantilever is in its “glassy stable” and it is unable to change shapes with an applied actuation magnetic field ( $B_a$ ). After the  $Fe_3O_4$  particles are heated up under an AC magnetic field ( $B_h$ ) (Figure 1b), the SMPs are into the “rubbery state”. So, the cantilever can change shape respective to the magnetic direction of  $B_a$  (Figure 1b). Once the temperature decreases back to room temperature (Figure 1c), the cantilever locks its shape without any external magnetic field applied.

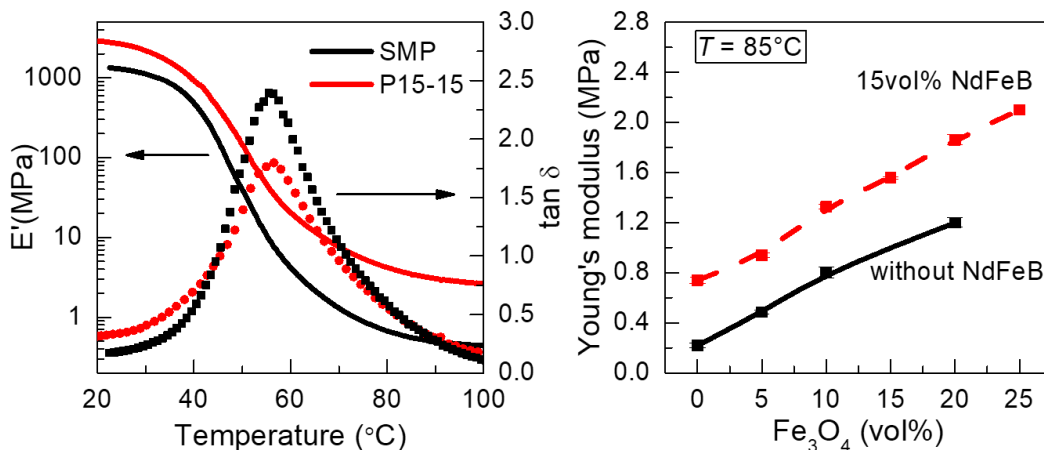


Figure 2 Thermomechanical of M-SMP<sup>1</sup>

Figure 2 shows the thermomechanical property of the neat SMP and M-SMP P15-15 (15% volume fraction of  $\text{Fe}_3\text{O}_4$  particles and 15% volume fraction of NdFeB particles). The glass transition temperature  $T_g$  can be measured as the temperature at the peak of  $\tan \delta$  which is around  $55^{\circ}\text{C}$ . With an increasing temperature from  $20^{\circ}\text{C}$  to  $100^{\circ}\text{C}$ , The storage Modulus of the SMP and M-SMP P15-15 decrease from 1.30GPa and 2.60GPa to 0.3Mpa and 2.8Mpa. The changing of Young's Modulus is tremendous under an increasing temperature. The M-SMP is stiff enough for holding heavy loads at a low temperature and is soft enough for actuating at a high temperature. The Young's Modulus of the M-SMP increases linearly with increasing loading of volume fraction of  $\text{Fe}_3\text{O}_4$  at  $85^{\circ}\text{C}$ . (Figure 2b) So, it is easy to control Young's Modulus difference caused by different volume fractions of the  $\text{Fe}_3\text{O}_4$  particles.

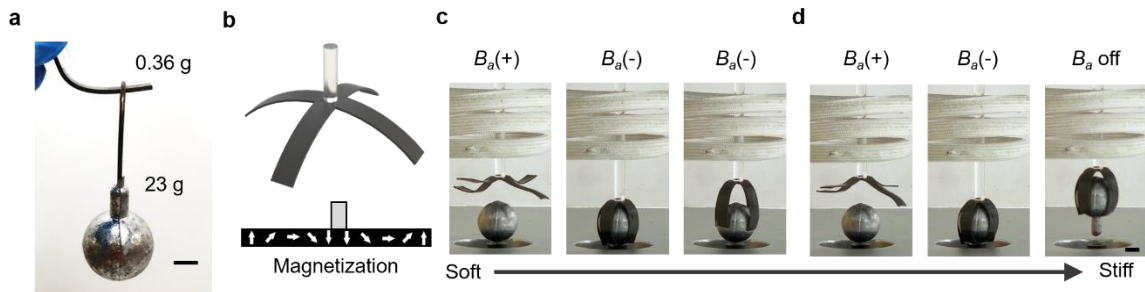


Figure 3 Physical property and application of M-SMP (scale bars: 5mm)<sup>1</sup>

Under room temperature, a cantilever made by M-SMP can hold a metal ball with a weight of 23g that is 60 times higher than the body weight, 0.36g, of the cantilever (Figure 3a). A four-arm robotic gripper is designed with M-SMP base on the physical property of M-SMP. The detailed magnetization of the grip is shown in figure 3b. At high temperature with a positive actuation magnetic field  $B_a$ , the gripper opens its four arms and ready for gripping. Then, the gripper successfully achieves gripping by switching the direction of the magnetic field to the negative direction. However, the gripper is still very soft that cannot hold the ball while lifting. (Figure 3c) After decreasing the temperature after gripping, the gripper locks its gripping shape. While lifting the gripper, the gripper can lift the lead ball without any applied magnetic field. (Figure 3d)

## ***Objective***

The technology for manufacturing M-SMP has restrictions on the design. The existing technology is using a thermal curing method for curing M-SMP. The method requires researchers to design the mold for the liquid phase M-SMP which limits the design of M-SMP structure to simple geometries. Also, due to the fabrication limitations, it is hard to design the multimaterial formed by both MSM and M-SMP. To overcome the limitations, we change the manufacturing method to be 3D printing and add photoinitiators into the material to allow it to be photocured. We are a customized 3D printer (Figure 4), and the printing method is called Magnetic Multimaterial Direct Ink Writing ( $M^3DIW$ ) technique. Use this technology, we are now capable of creating more complex structures with much smaller dimensions.

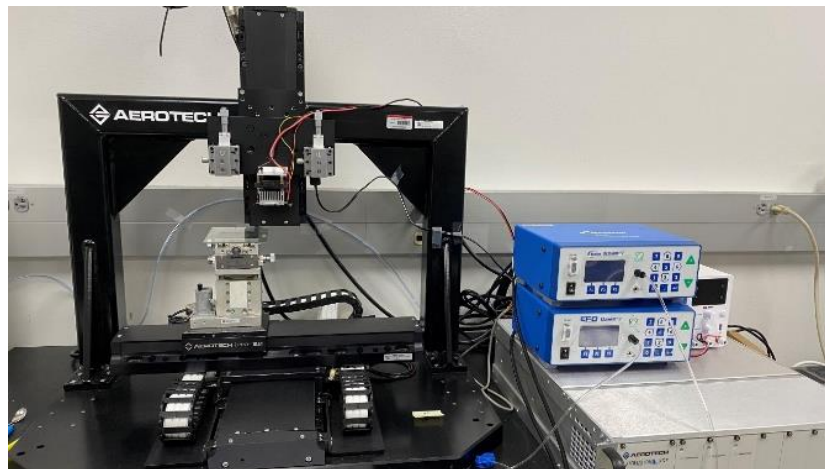


Figure 4 Customed 3D printer for  $M^3DIW$

## ***Methodology***

M-SMP and MSM are composed of different types of photocurable polymeric resins, magnetized Neodymium-Iron-Boron (NdFeB) particles, photoinitiator, and fumed silica nanoparticles. The polymeric resin for M-SMP contains Isobornyl Acrylate (IOA) and 2-Phenoxyethanol Acrylate (PEA). The polymeric resin for MSM contains PEA and Isodecyl Acrylate (IA). Both resins contain a cross-linker called Aliphatic Urethane Diacrylate (AUD). The difference of resins' components leads to different performances under room temperature. NdFeB particle is a high-remanence and high-coercivity magnetic particle. Once it is magnetized, it maintains an internal magnetization that can be controlled by an external magnetic field. M-SMP also contains Iron(II, III) Oxide( $\text{Fe}_3\text{O}_4$ ) particles for heating purposes. Not like the NdFeB particle,  $\text{Fe}_3\text{O}_4$  particle cannot be magnetized, which minimize its impact on actuation under an external magnetic field. To overcome the limitations caused by the thermal curation, we add a photoinitiator in both M-SMP and MSM that both materials can be cured under an ultraviolet (UV) LED light. During the manufacturing procedure, Silica particles are added because they can increase the viscosity of the materials, which allows materials to stay in shape at their liquid phase.

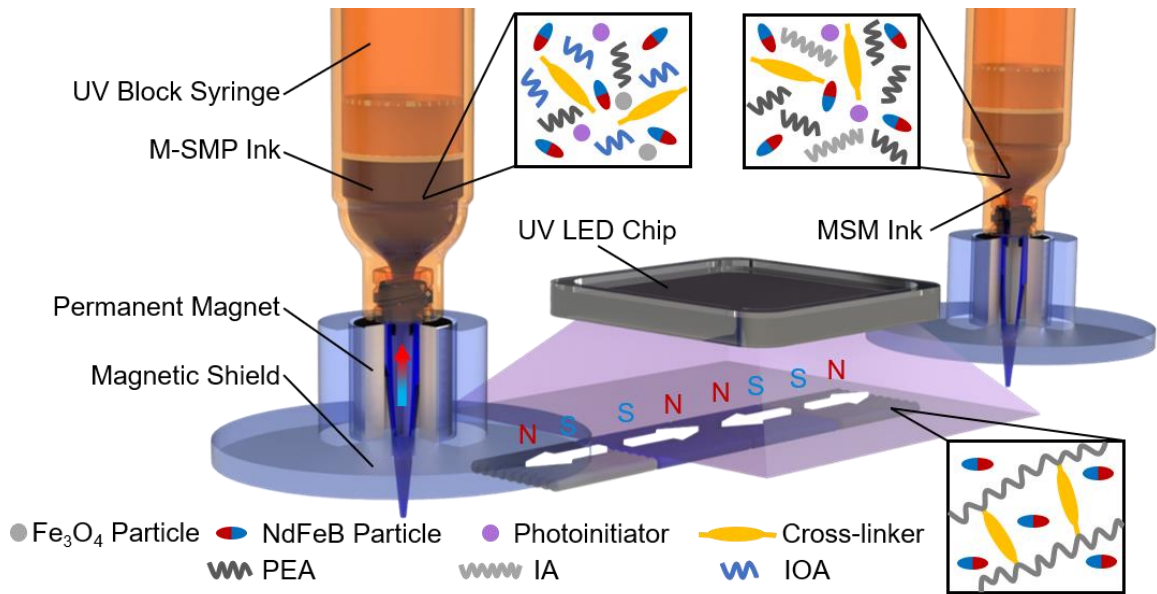


Figure 5 Magnetic multimaterial direct ink writing (M<sup>3</sup>DIW)<sup>2</sup>

In this research, we introduce a new 3D printing technique called magnetic multimaterial DIW(M<sup>3</sup>DIW). (Figure 5) The magnetized M-SMP ink and MSM ink are placed inside syringes and the syringes are UV block syringes that are used to prevent inks cured before printing. Permanent magnets are fixed on the nozzles to align the magnetized direction of the magnetic particles with a magnetization direction pointing up. So, the magnetized direction of the printed material can be controlled by the motion of the 3D printer during printing. The magnetic shields are used to protect the printed material from permanent magnets. A UV LEP chip is utilized for curing the printed material. In this case, M-SMP enters its “glassy state” and MSM enters its “rubbery state”.

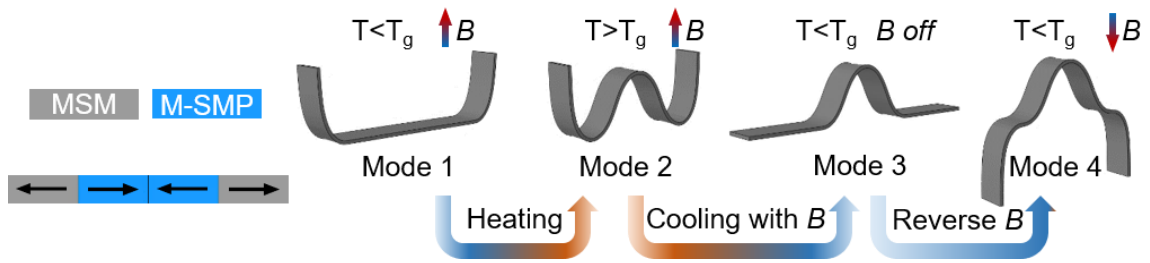


Figure 6 Working mechanism of the multimaterial (MSM&M-SMP)<sup>2</sup>

Figure 6 shows a working mechanism of a one-dimensional M-SMP/MSM composites structure. The gray color represents MSM and the blue color represents M-SMP. Their magnetization directions are labeled under their color. With the temperature lower than M-SMP's  $T_g$  (glass transition temperature), only MSM will be actuated under a magnetic field, forming the actuator into a "U" shape. (Mode1) Once the temperature is above  $T_g$ , both materials actuated by the applied magnetic field, forming the actuator into a "W" shape. (Mode2) After cooling down to room temperature and removing the magnetic field, MSM parts back to their original shape but M-SMP parts become stiff and lock themselves into a mountain-like shape. (Mode3) Finally, MSM parts achieve a shape-changing under a reverse magnetic field when M-SMP parts remain the shapes because of their high stiffness. (Mode 4) Therefore, MSM and M-SMP have different performances under different temperatures, we utilize these properties for creating complex structures that have multiple shapes with one design.

## Result

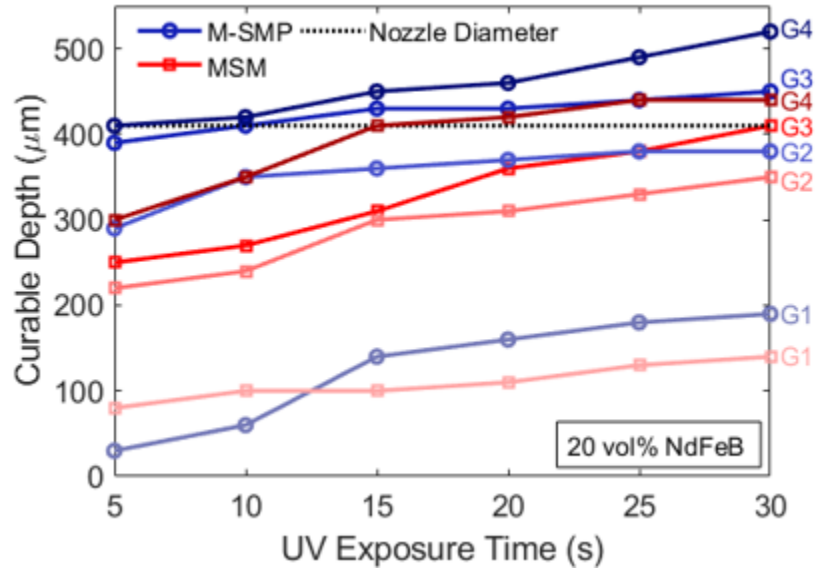


Figure 7 Curable depth vs. UV exposure time for different NdFeB particle sizes<sup>2</sup>

To create a stable printing environment, the NdFeB particle sizes with a suitable curable depth are selected based on the experiment. Initially, there are four different particle sizes:  $22.5 \pm 7.5 \mu\text{m}$  (G1);  $37 \pm 6 \mu\text{m}$  (G2);  $58 \pm 16 \mu\text{m}$  (G3);  $112 \pm 38 \mu\text{m}$  (G4). Figure 7 shows the changing curable depth of the material with 40% volume fractions of NdFeB to the UV exposure time. It clearly shows that the longer time that the materials expose under the UV light, the more material is cured. During printing, the material extruded from the nozzle, which has a diameter of  $410 \mu\text{m}$ , on the substrate. The thickness of the layer created on the substrate is close to the diameter of the nozzle. So, the desired curable depth should be larger than the nozzle's diameter. From figure 13, only NdFeB particle sizes G3 and G4 have a reasonable curable depth under the UV light



for 30 seconds. NdFeB particle size G2 is close to the diameter of the nozzle. However, NdFeB particle with sizes G3 and G4 can form large clusters after magnetization that contains a high risk for causing clogging during the printing. The NdFeB particle size G2 is selected. To increase the curable depth for inks with NdFeB particle size G2, the volume fraction of NdFeB particle is decreasing to 15%.

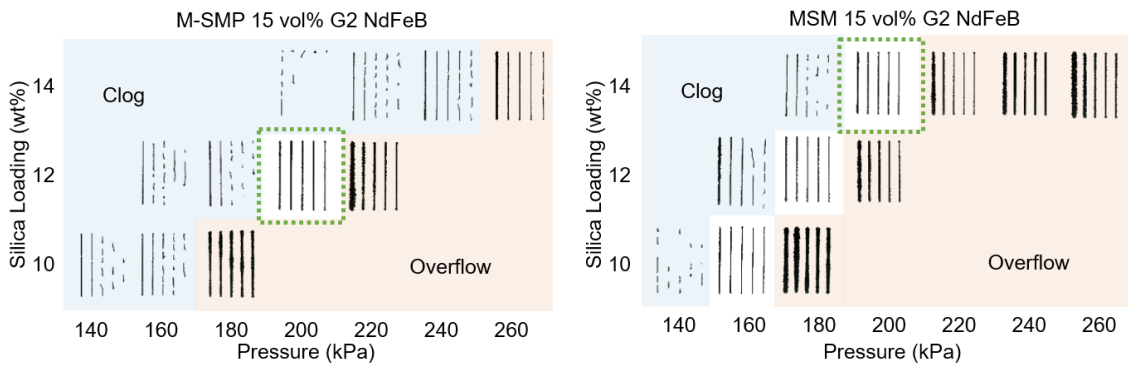


Figure 8 Printing qualities for both materials with different silica loading and pressure<sup>2</sup>

With a fixed 15 vol% NdFeB particles with G2 size, silica loading and extruding speed can significantly change the printing qualities. (Figure8) Because of the unique printing technique (M<sup>3</sup>DIW), the extruding speed is controlled by the input pressure. A low weight fraction of silica loading with a high input pressure can cause printed ink overflow. A high weight fraction of silica loading with a low input pressure can clog the nozzle during printing and create a discontinuous printed ink on the substrate. To achieve the best printing qualities for M-SMP, it requires a 12% weight of silica loading and a

200kPa input pressure during printing. For MSM, three different silica loadings reach our desired printing qualities. However, MSM with a weight percentage of silica loading lower than 14% can cause phase separation of the resin and NdFeB particles, the MSM requires a silica loading with 14% weight of ink and under an input pressure 200kPa during printing.

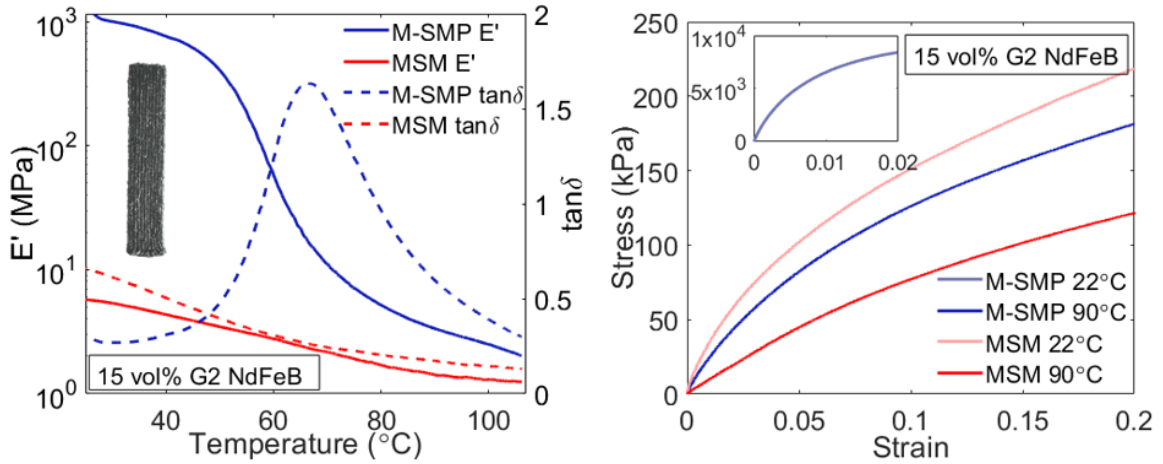


Figure 9 Thermomechanical property of MSM and M-SMP<sup>2</sup>

A thin-film specimen is successfully printed using our M<sup>3</sup>DIW printing technique for dynamic mechanical analysis testing. (Figure 9) The  $T_g$  is measured as the temperature at the peak of  $\tan \delta$  which is around 66°C. As the temperature increases from 20°C to 100°C, the storage modulus of M-SMP and MSM drops from 1.16GPa and 5.75MPa to 2.02MPa and 1.24MPa, respectively. M-SMP has a large decrease of the storage modulus when the temperature increases that allows it to transfer from its glassy state to its rubbery state. The graph in the right of figure 15 shows the tensile test results of both materials at temperatures 22°C and 90°C. From the graph, clearly shows that M-SMP at 22°C has a much higher Young's modulus than the other three conditions. The Young's

moduli of M-SMP at 22°C and 90°C are 1.16GPa and 2.04MPa, and Young’s moduli of MSM at 22°C and 90°C are 1.64MPa and 0.89MPa.

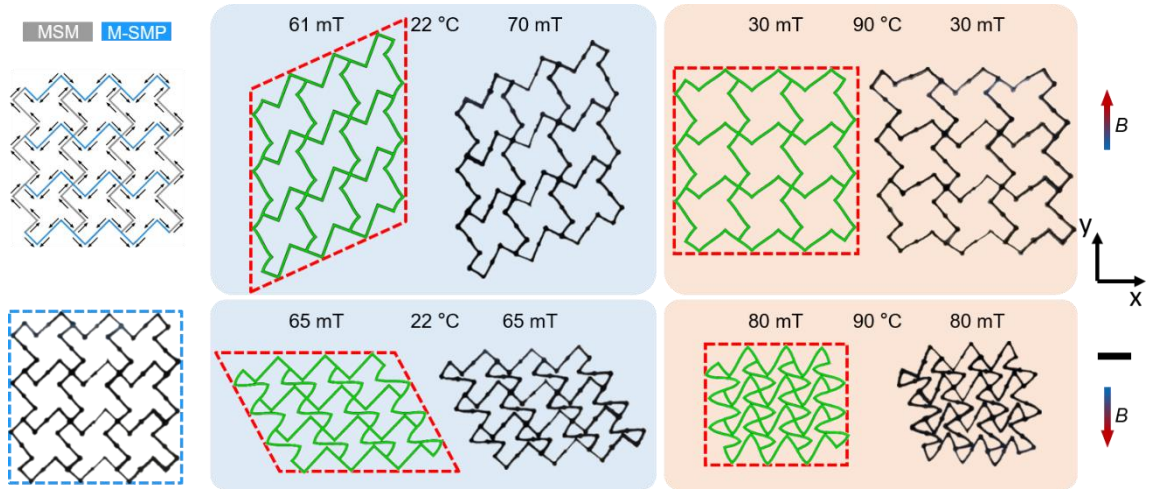


Figure 10 The working mechanism of a 2D chiral design with MSM/M-SMP (scaler bar: 10mm)<sup>2</sup>

A two-dimensional chiral design is structured by both MSM and M-SMP (Figure 10). The schematic of the design is shown in the top right corner with MSM (gray) and M-SMP (blue) connected. The magnetization directions are also shown next to their materials. The actual printed structure is shown in the bottom right corner. In figure 10, all the actual actuation of the designs are shown to the right of their schematics. At 22°C, the M-SMP parts are stiff that do not have shape-changing under the magnetic field. However, MSM can change the shapes by increasing or decreasing their connecting angle under the two different directions of the actuation magnetic field. So, the structure performs two different shear deformations with a positive Poisson’s ratio. When the

temperature reaches 90°C, both materials into their rubbery states. All parts of the chiral design are actuated under an actuation magnetic field. When applying an actuation magnetic field to the positive y-direction, the chiral design expands its structure because of the increase of all the connected angles and performs biaxial expansion. Under a reversed magnetic field, the chiral design shrinks its structure, when all the connected angle decreases and performs a biaxial contraction. The design at 90°C gives us a negative Poisson's ratio. Due to the properties of MSM and M-SMP, the chiral design has a total number of five different shapes under different temperatures and magnetic fields.

To increase the functionality of the multimaterial designs, we further analyzed a unique type of structure called Kresling origami. It is successfully constructed as a soft robot that has huge potential for carrying the multimaterial designs for more functionality in many applications.

# Magnetic origami robot

## *Introduction*

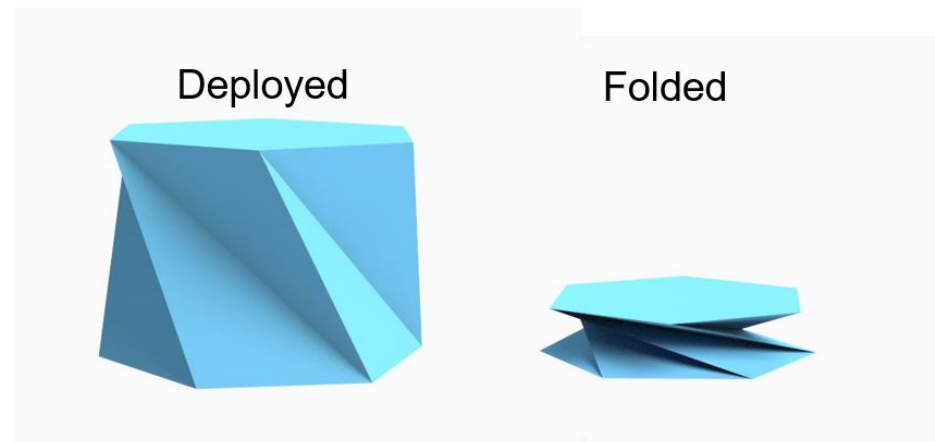


Figure 11 Geometry of Kresling origami

The paper folding art, Origami, has been using in many engineering applications such as aerospace, civil, and soft robotic because of its foldability and multifunctionality. Here we introduce a unique pattern of origami called Kresling Origami. (Figure11) Kresling origami is designed with two plain pieces parallel to each other and connected by multiple triangle pieces of equal sizes. It has two different states: deployed state and flat-folded state. To achieve a transformation between the two states requires a rotation between the two parallel pieces. Note that the applied rotational torque needs to overcome an energy barrier to fully transfer from deployed state to the flat-folded state. Once the

torque reaches the peak of the energy barrier, the Kresling unit cell will accomplish its shape transformation in a tenth of a second. However, there is a smaller energy barrier from the flat-folded state to the deployed state. The difference caused the deployed state to have higher stability than the folded state. The magnitude of the energy barrier is depending on the using material and the Kresling origami geometry. Generally, a Kresling origami design created by a higher Young's Modulus material with a larger height has a higher energy barrier than that created by a lower Young's Modulus material with a lower height.

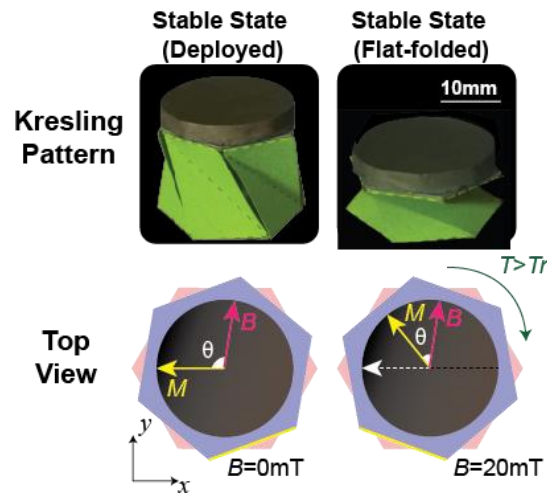


Figure 12 Magnetic actuation of the magnetic Kresling unit cell<sup>3</sup>

Now, remote control of the transformation of the Kresling origami has been achieved. It is structured by fixing one side of the Kresling origami on board and placing a magnetic-responsive plate on the other side. (Figure12) The plate is created by a type of polymer resin called Ecoflex ( 00-30 silicone rubber) with NdFeB particles and it has been magnetized in-plane under an impulse magnetic field before placing on the Kresling

Origami. It allows the magnetic Kresling unit cell control untethered by an external magnetic field. Under the external magnetic field  $B$ , a torque  $T$  is generated based on the equation  $T = VM\sin(\theta)$ , where  $M$  is the magnetization of the disc,  $V$  is the volume of the disc, and  $\theta$  is the angle between  $M$  and  $B$ . To create a large enough torque, the initial  $B$  is set with an angle difference around  $90^\circ$  with the magnetization direction of the plate. (Figure 12, Top View) Once the magnetic field is applied, a torque  $T$  is produced to overcome the required torque  $T_r$ , generated by the geometry of Kresling origami, for fully state transformation. If  $T$  is larger than  $T_r$ , the magnetic Kresling unit cell can transfer from its deployed state to its folded state.

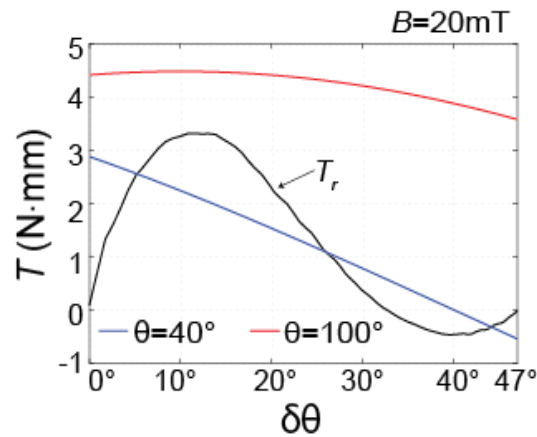


Figure 13 Magnetic torque vs. plate rotation angle

Figure 13 shows a relationship between the torque  $T$  and the rotation angle of the plate  $\delta\theta$  of the magnetic Kresling unit cell from deployed state to the folded state. It also shows the magnitude of the required torque  $T_r$  at different rotation angles. The peak of the  $T_r$ , at around  $12^\circ$ , is the maximum that is needed for state transformation. So, the magnetic Kresling unit cell is staying its deployed state until the applied torque is higher

than the peak. Under a fixed direction and 20mT magnetic field with a plate with a fixed value of  $M$  and  $V$ , the magnitude of torque is only depending on the angle  $\theta$ . During the folding procedure, the  $\delta\theta$  increases, which the angle  $\theta$  decreases that causes the torque to have a downward shifting. (Figure 13) Therefore, to transfer the magnetic Kresling unit cell from its deployed state to its folded state, the initial value of angle  $\theta$  needs to be large enough to allow enough applied torque higher than the peak of  $T_r$  at the specific  $\delta\theta$ .



## ***Methodology***

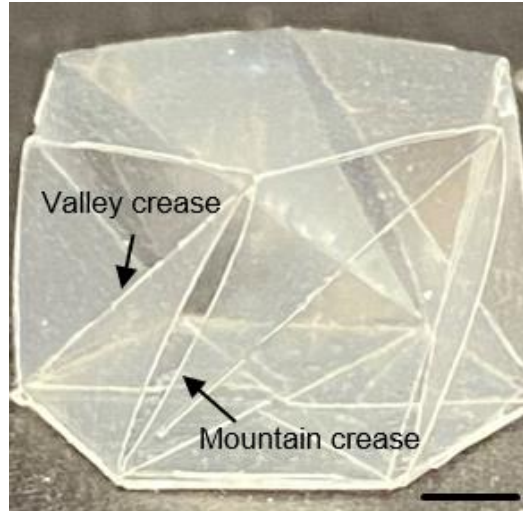


Figure 14 The geometry of Kresling origami (scaler bar: 5mm)

Besides the improvement on the multimaterial manufacturing, the complex structure, Kresling origami, has also been studied and expanded its functions. In this research, two types of magnetic Kresling robots were designed and manufactured base on the analysis of the magnetic Kresling unit cell. The first type of magnetic Kresling robot can achieve multidirectional swimming motions in water and the second type of magnetic Kresling robot is capable of swimming in a horizontal direction with a drug-release function. To achieve the functions of both designs, we add some changes to the Kresling origami structure. (Figure 14) The mountain crease of the Kresling origami is cut through. The valley crease that connects two triangles gets two cuts on the crease and is left with only one small crease in the middle and two small creases in the corners. The material changes to Polyethylene with a Young's Modulus of 1577.9MPa. All these changes caused

a geometry property shift of the Kresling origami from bi-stable to monostable. It allows the Kresling origami to have its deployed state as its natural state with a capability of folding by a relatively small rotational torque.

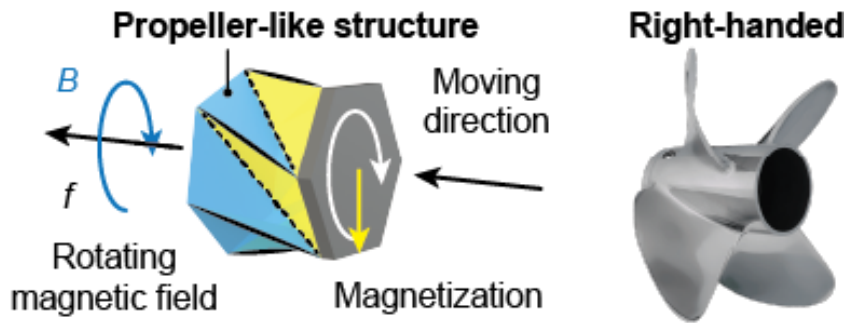


Figure 15 Magnetic Kresling robot and a right-handed propeller schematic

Compare the structure of Kresling origami with a propeller (Figure 15), the Kresling origami contains a propeller-like structure. Since the magnetic disc has an in-plane magnetization, under a rotating magnetic field  $B$ , the magnetic Kresling robot is capable of rotating in the same direction as the magnetic field. Due to the geometry of the Kresling Origami, the moving direction of the magnetic Kresling robot is always perpendicular to the disc surface. The working mechanism is shown in Figure 15. Under a clockwise rotating magnetic field, the magnetic Kresling robot rotates clockwise with a moving direction to the right. The moving force is created by the parts of geometry that are covered by the blue color. They create several force components to form the driving force by pushing the water backward and allow the magnetic Kresling robot to swim in the desired direction.

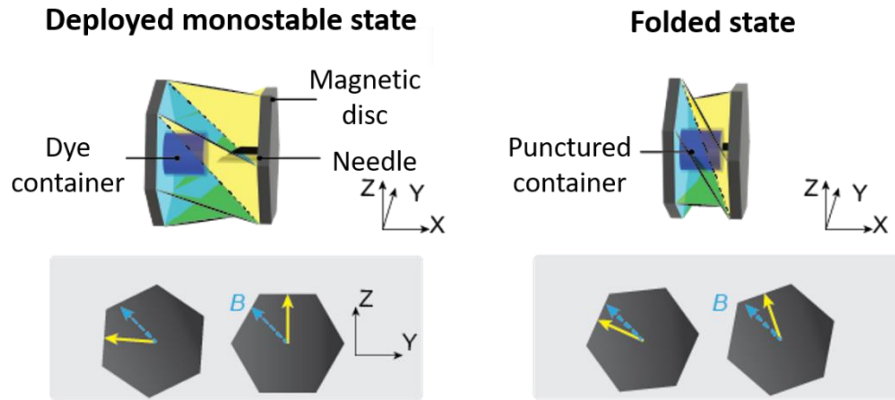


Figure 16 Magnetic Kresling robot with drug-release function

Figure 16 shows the structure and working mechanism of the magnetic Kresling robot with drug-release function. The magnetic Kresling robot is capable of swimming to the target position and releasing the contained drug. Two magnetized discs are placed on both sides of the Kresling origami structure. A dye container is placed inside of the magnetic Kresling robot and fixed on one side of the inner surface of the disc. It fully contains a blue color dye and is sealed by parafilm. A needle is placed on the other side of the inner surface and points at the center of the dye container. At the magnetic Kresling robot's deployed state, an approximate 2mm distance is fabricated between the sharp point of the needle and the dye container. Once the magnetic Kresling robot is folded, the needle puncture through the parafilm on the dye container and releases the dye into the water to achieve drug release. To accomplish the folding process, an angle changing is needed between the two magnetic discs' in-plane magnetized direction. After applying a fixed directional magnetic field in the same plane as the disc's surfaces, the magnetic Kresling robot automatically rotates to the desired angle. (Figure 16) The angles between

the two magnetized directions of the discs (yellow) and the direction of the magnetic field (blue) are the same. Then the magnetic field forces the two discs to rotate in the opposite direction to reach the folded state and accomplish drug release. Once the magnetic field is released, the magnetic Kresling robot back to its deployed state simultaneously.

## Result



Figure 17 Magnetic Kresling robot swims in the horizontal direction (scaler bar: 13mm)

Figure 17 shows a demonstration of the magnetic Kresling robot swimming in the horizontal direction. An external magnetic field with 10mT magnitude and 15Hz rotating frequency is applied on the same plane as the surface of the magnetic disc (40vol% of NdFeB particles) on the magnetic Kresling robot. It creates a constant angular velocity on the magnetic disc that causes a moving force on the magnetic Kresling robot to swim in the positive x-direction.

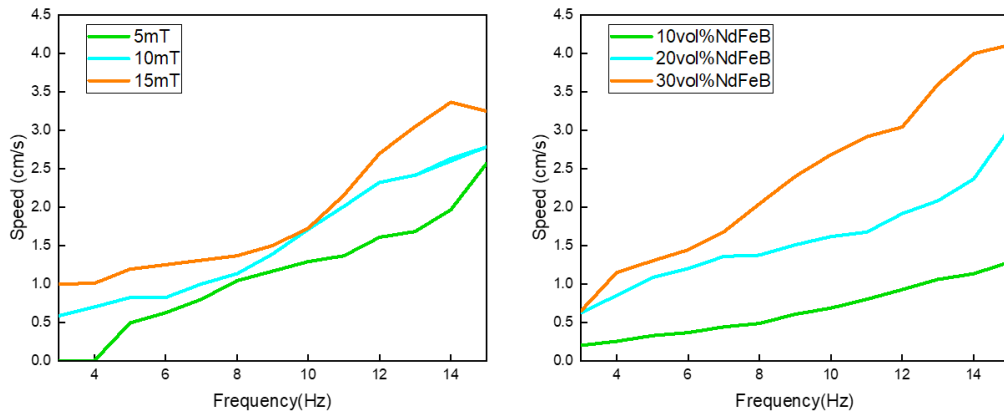


Figure 18 Speed vs. input frequency for different conditions for horizontal swimming

The dynamic motion results for horizontal swimming are shown in figure 18. With the same NdFeB volume fraction of the magnetic disc, increasing the input frequency of the magnetic field can increase the swimming speed of the magnetic Kresling robot. A higher frequency input allows the magnetic disc has a higher rotating frequency, which creates a larger moving force for the magnetic Kresling robot. Because of the existence of friction and other unwanted forces, the actual rotating frequency of the magnetic disc is lower than the input rotating frequency. A higher magnitude of the input magnetic field, however, can help the magnetic disc to have a better match with the rotating frequency. Therefore, under the same input frequency and NdFeB particles volume fraction, an input magnetic field with 15mT can produce a faster speed for the magnetic Kresling robot than an input magnetic field with 5mT can do. Under the same magnitude, magnetic discs with higher NdFeB particles volume fraction can form a higher motion speed for the magnetic

Kresling robot. Since weight is not directly dragging the swimming motion of the robot, a higher magnetic particles volume fraction can create a higher torque on the magnetic disc by following the equation  $T = VM\sin(\theta)$ . Thus, under the same input frequency and magnitude of the magnetic field, a 30vol% disc is creating a higher speed for the robot than a 10vol% disc. (Figure 18)

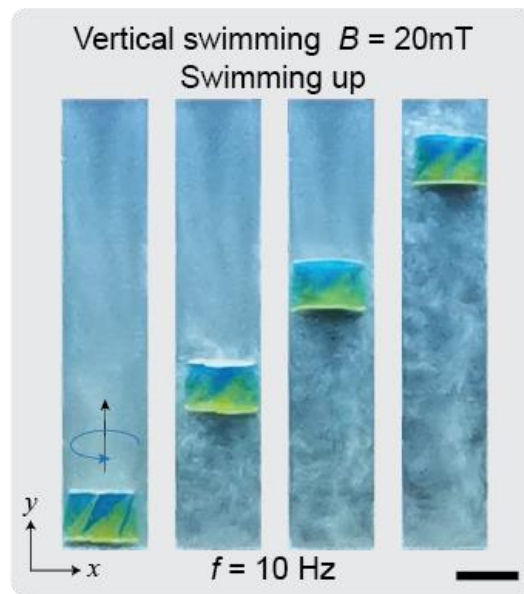


Figure 19 Magnetic Kresling robot swims in the vertical direction (scaler bar: 13mm)

For vertical swimming, the NdFeB particles volume fraction of the disc is around 3%. The magnetic Kresling robot needs to overcome its gravity force for vertical motion swimming. A magnetic Kresling robot with a 3vol% magnetic disc is capable of swimming vertically under a 20mT magnetic field with a 10Hz input rotating frequency. (Figure 19) A much lower magnetic particle volume fraction allows the robot to enough torque on its magnetic disc to produce a driving force to overcome its gravity force.

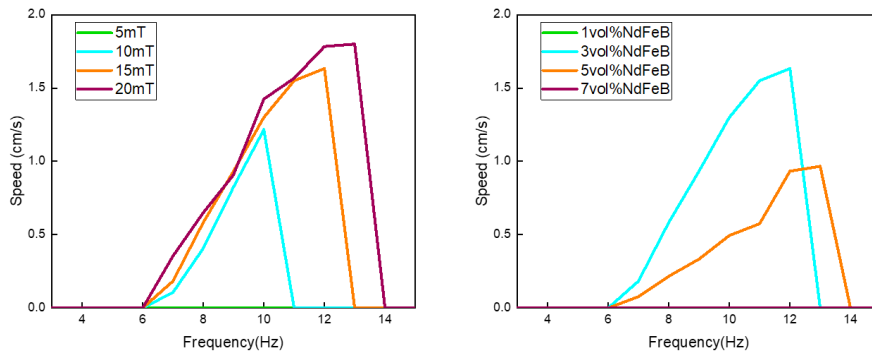


Figure 20 Speed vs. input frequency for different conditions for vertical swimming

Figure 20 shows the dynamic motion performance of the magnetic Kresling robot in vertical swimming. Under the same magnetic particle volume fractions, after overcoming the gravity force of the robot, which needs an input rotating frequency to be higher than 6Hz, the swimming speed of the robot increases as the input rotating frequency increases, until the magnetic discs cannot match the input rotating frequency. (Figure 20) This is caused by the leak of torque due to a low magnetic particle volume fraction. It is also explained by figure 5e that a higher magnitude of the magnetic field can provide a higher speed for the robot at higher input rotating frequency. Besides, because of the lightweight of the robot, once the rotating frequency of the magnetic disc matches the input rotating frequency, the speeds of the robot have a small difference under the same input rotating frequency. Figure 5f shows the significant influence on the robot's vertical swimming performance. When the NdFeB particles volume fraction is too low (1vol%) the driving force created by the torque on the magnetic disc is lower the weight of the robot that the robot cannot perform a vertical swimming motion. When the NdFeB



particles volume fraction is too high (7vol%) the weight of the robot is too high which caused the same result as a low NdFeB particles volume fraction. From the experiment results, the magnetic Kresling robot with a 3vol% magnetic disc can perform the highest speed of motions under the same magnitude and input rotating frequency on the magnetic field.

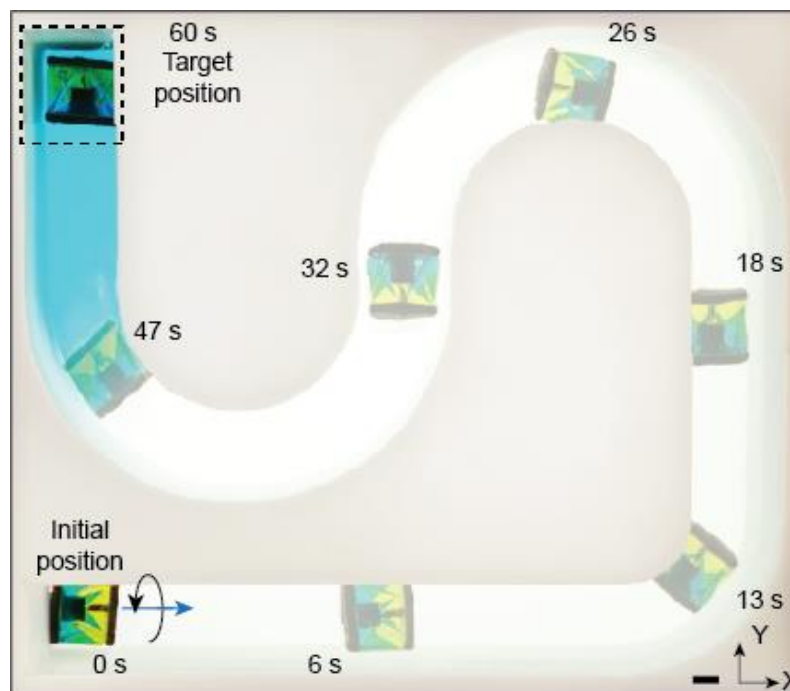


Figure 21 Magnetic Kresling robot travels in maze and drug released (scaler bar: 8mm)

The magnetic Kresling robot with drug-release function is capable of traveling in a simple maze and achieve drug release at the target position. (Figure 21) With an applied counter-clockwise rotation magnetic field in the YZ plane, the robot starts spinning in the same rotation direction and swims to the positive x-direction. By changing the plane angle of the magnetic field in the XY plane, the robot turns direction that respect to the

changing angle. Once the robot reaches the target position, a fixed one-dimensional magnetic field forces the robot to fold and accomplish drug release.

## Conclusion

Using the Magnetic Multimaterial DIW printing technique, both MSM and M-SMP can be constructed together to form into different complex designs. Both MSM and M-SMP are composited with 15% volume fractions of NdFeB particles with size  $37 \pm 6 \mu\text{m}$ . To maximum the printing quality, MSM needs to contain 14% weight fractions of silica loading with a constant input pressure of 200kPa and M-SMP needs to contain 12% weight fractions of silica loading with the same amount of input pressure. In this research, a chiral structure is a design with MSM and M-SMP. Because of the property difference of the MSM and M-SMP, the chiral design has a total of 5 different shapes under different magnetic fields and temperatures. The chiral design is only one example of the M<sup>3</sup>DIW results. It shows the tremendous potential that M<sup>3</sup>DIW has for manufacturing complex structures with small dimensions.

The magnetic Kresling robots have the great capability of performing swim remotely. The magnetic Kresling robot with one disc can achieve both horizontal swimming and vertical swimming. With a higher input angular frequency, the magnetic Kresling robot can swim faster under the same magnetic field. The magnitude of the magnetic field is used to match the actual angular frequency of the robot with the input angular frequency. With a higher value of the magnetic field, the robot can reach a higher angular frequency which tends to have a higher speed. The magnetic Kresling robot with

drug-release function can accomplish swim in a simple maze and release drugs at the target position.

Both multimaterial designs and magnetic Kresling robots have multiple functions. Adding a unique design with multimaterial on the magnetic Kresling robot has great potential for inventing robots with exhaustive functions in the future.

## **Bibliography**

[1] Ze, Q.#, Kuang, X.#, Wu, S.#, Qi, H.J., Zhao, R. et al. *Advanced Materials* 32.4 (2020): 1906657.

[2] Ma, C.#, Wu, S.#, Qi, H. J., Zhao, R. et al. *ACS Applied Materials & Interfaces* (2020).

[3] Novelino, L.S.#, Ze, Q.#, Wu, S.#, Paulino, G.H. Zhao, R. *Proceedings of the National Academy of Sciences* 117.39 (2020): 24096-24101.